Supplementary Information for

A "Seat-squatting" Strategy via Lithium Substitution to Suppress Fe-Migration in Na layered Oxide Cathode

Yaoshen Niu[1,2], Zilin Hu[1], Huican Mao*[3], Lin Zhou[1], Liguang Wang[4], Xiaobing Lou[5], Bo Zhang[6], Dongdong Xiao[1], Yang Yang[1], Feixiang Ding[1], Juping Xu[7], Wen Yin[7], Nian Zhang[8], Zhiwei Li[6], Yaxiang Lu[1], Xiaohui Rong*[9], Bingwen Hu[5], Jun Lu[4], Ju Li*[10], Yong-Sheng Hu*[1]

[1]Key Laboratory for Renewable Energy, Beijing Key Laboratory for New Energy Materials and Devices, Beijing National Laboratory for Condensed Matter Physics, Institute of Physics, Chinese Academy of Sciences, The College of Materials Sciences and Opto-Electronic Technology, University of Chinese Academy of Sciences, Beijing 100190, China

[2]Frontier Institute of Science and Technology, Xi'an Jiaotong University, Xi'an 710049, China

[3]Department of Energy Storage Science and Engineering, School of Metallurgical and Ecological Engineering, University of Science and Technology Beijing, Beijing 100083, China

[4]Chemical Sciences and Engineering Division, Argonne National Laboratory, Lemont, IL, USA.

[5]Shanghai Key Laboratory of Magnetic Resonance, State Key Laboratory of Precision Spectroscopy, School of Physics and Electronic Science, East China Normal University, Shanghai 200241, P. R. China

[6]Key Lab for Magnetism and Magnetic Materials of the Ministry of Education, Lanzhou University, Lanzhou 730000, China

[7]Spallation Neutron Source Science Center, Dongguan 523803, China

[8]State Key Laboratory of Functional Materials for Informatics, Shanghai Institute of Microsystem and Information Technology, Chinese Academy of Sciences, Shanghai 200050, People's Republic of China.

[9]Yangtze River Delta Physics Research Center Co. Ltd; Liyang, 213300, China.

[10]Department of Nuclear Science and Engineering and Department of Materials Science and Engineering, MIT, Cambridge, MA 02139, USA

*Corresponding authors. Email: hcmao@ustb.edu.cn (Huican Mao) rongxiaohui@ioply.cn (Xiaohui Rong), liju@mit.edu (Ju Li) yshu@iphy.ac.cn (Yong-Sheng Hu)

Supplementary information

Table of contents

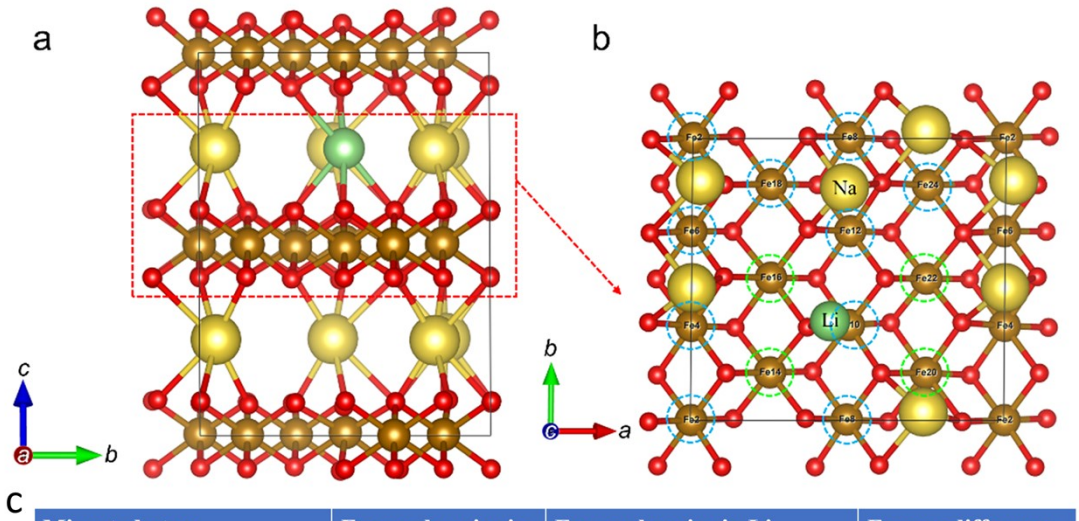

Migrated atom	Energy barrier in $Na_{0.33}FeO_2$ (eV)	Energy barrier in Li-substituted $Na_{0.33}FeO_2$ (eV)	Energy difference ΔE (eV)
Fe22 (shown in manuscript)	-2.25	-1.41	0.84
Fe8	-1.61	0.59	2.20
Fe12	-1.90	-0.19	1.71

Fig. S1. (a) The crystal structure of Li-substituted $Na_{0.33}FeO_2$, with a Na-layer containing a Li ion and TM-layer plotted in the red dashed rectangle. (b) The local structure of the Na (containing a Li ion)-TM layer (plotted in the red dashed rectangle) projected along the c-direction. (c) Comparison of the energy barriers for Fe22, Fe8, and Fe12 atoms as marked in Fig. S1b, where Fe22 represents the case without considering Li-induced changes in Fe valence states, while Fe8 and Fe12 represent cases with Li-induced local changes in Fe valence states. The energy barrier for Fe migration from an octahedral site in the TM layer to a tetrahedral site in the Na layer of $Na_{0.33}FeO_2$ and Li-substituted $Na_{0.33}FeO_2$ is labeled as "Energy barrier in Na0.33FeO2" and "Energy barrier in Li-substituted $Na_{0.33}FeO_2$," respectively. The difference in energy barriers between migrating Fe atoms in $Na_{0.33}FeO_2$ and Li-substituted $Na_{0.33}FeO_2$ is labeled as "Energy difference ΔE."

To investigate the impact of the extra Li atom in alkaline layer to the average valence of Fe, we calculated the Bader charge of Fe ions based on C2/m $Na_{0.33}FeO_2$ and Li-substituted $Na_{0.33}FeO_2$ systems. Compared with $Na_{0.33}FeO_2$, we found that not all Fe ions'valence decreases in the Li-substituted $Na_{0.33}FeO_2$ system. Most Fe ions' valence states decrease, while a small fraction of Fe ions show a slight increase in valence, likely due to their local

structures. As shown in Fig. S1, for the Na (containing a Li ion)-TM layer, we observed that most Fe ions in the Li-substituted $Na_{0.33}FeO_2$ system have a lower oxidation state (marked with blue dotted circles) compared to those in $Na_{0.33}FeO_2$. However, several Fe ions exhibit an oxidation state higher by 0.1-0.2 (marked with green dotted circles). In Fig. 1 of the main text, Fe22 (with an increasing valence of Fe) was selected to characterize Fe migration for energy calculations. The energy barrier for Fe migration from an octahedral site in the TM layer to a tetrahedral site in the Na layer of $Na_{0.33}FeO_2$ is 0.84 eV lower than that in Li-substituted $Na_{0.33}FeO_2$. Additionally, similar calculations were conducted for Fe8 and Fe12 ions, which have decreasing valence. As shown in Fig. S1c, the energy barriers for Fe8 and Fe12 migration from an octahedral site in the TM layer to a tetrahedral site in the Na layer of $Na_{0.33}FeO_2$ are 2.20 eV and 1.71 eV lower, respectively, than those in Li-substituted $Na_{0.33}FeO_2$.

This suggests that Li^+ occupying the tetrahedral site in the Na layer raises the energy barrier for Fe migration, regardless of whether their oxidation state is increased or decreased, implying a reduced tendency for Fe migration in the presence of Li. Therefore, we surmise that alterations in the oxidation state of Fe have negligible influence on its migration. It is likely the crystallographic positions occupied by Li^+, along with the electrostatic repulsion between Li and Fe ions, that contribute to the impediment of Fe migration.

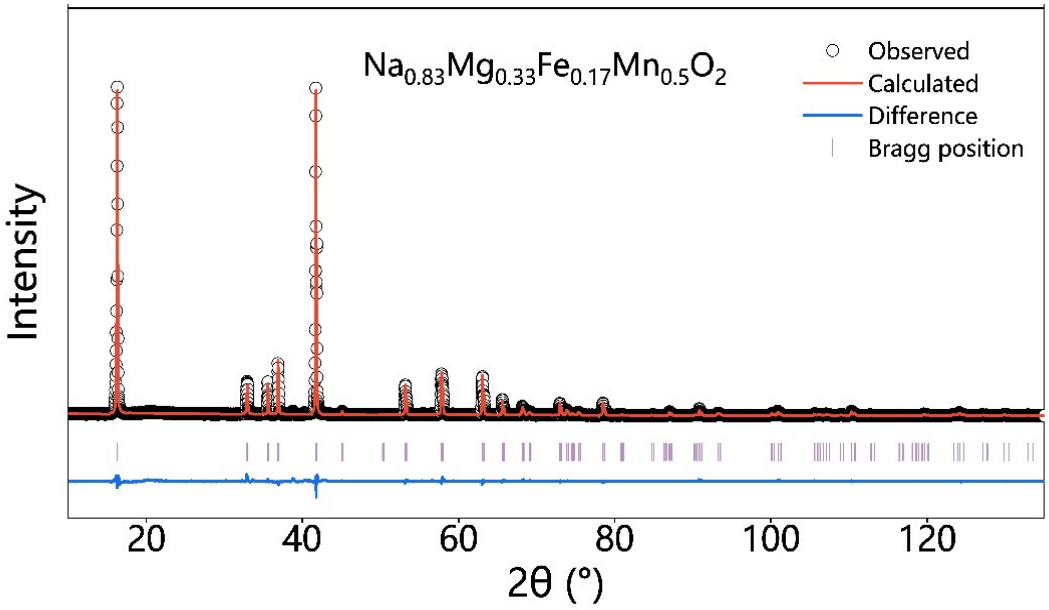

Fig. S2. Refined XRD patterns of synthesized O3-NaMFM samples.

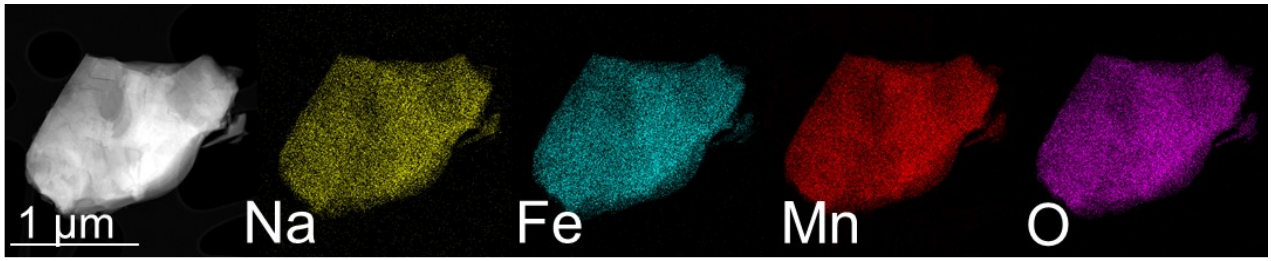

Fig. S3. EDS mappings of Na, Fe, Mn, and O elements.

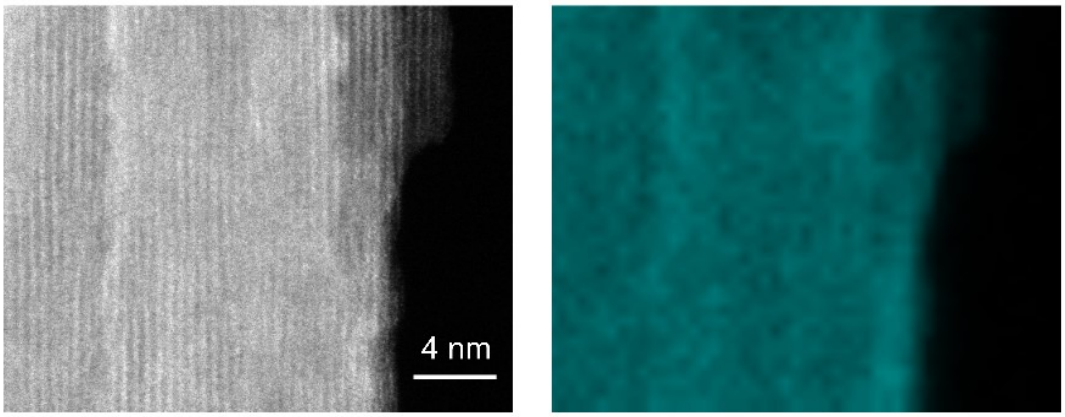

Fig. S4. STEM image (a) and corresponding EELS Li maps (b) of a nanoscale surface region in pristine NaLFM.

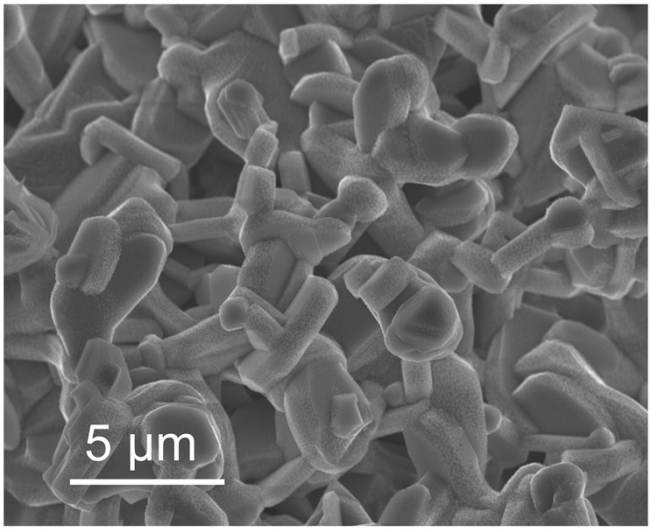

Fig. S5. SEM image of NaLFM.

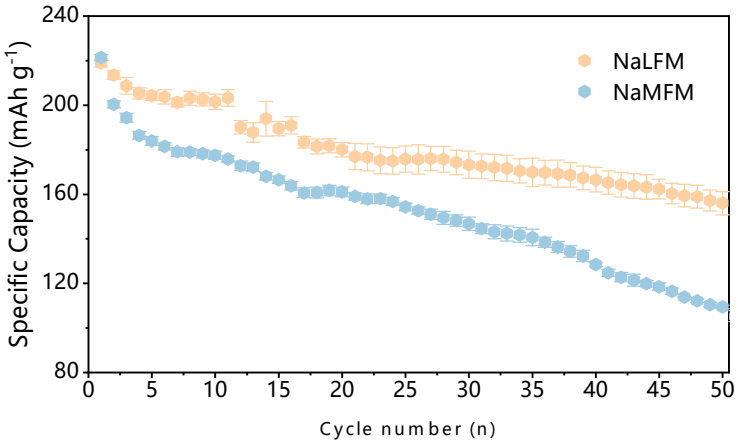

Fig. S6. Comparison of galvanostatic cycling performance of the half-cell at 10 mA g^{-1} within 1.5-4.5 V between O3-NaLFM and O3-NaMFM. Error bars: standard deviation of three cells for each sample.

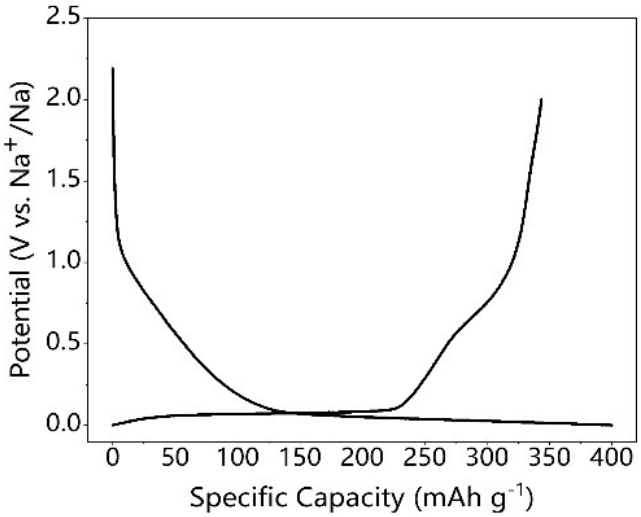

Fig. S7. Galvanostatic charge and discharge profiles of the Hard carbon at 20 mA g^{-1} between 0-2 V for the first cycle.

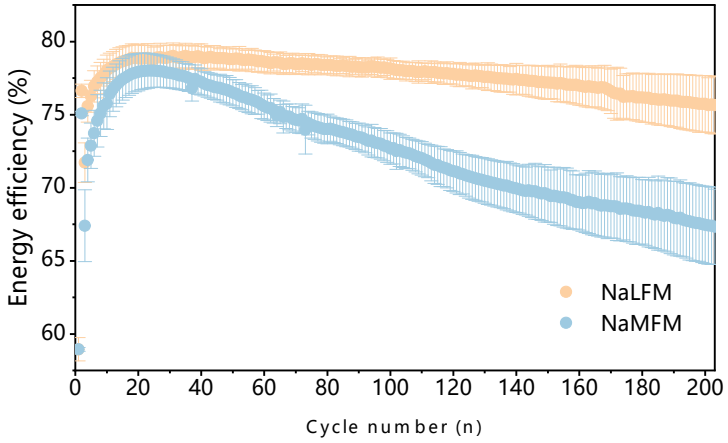

Fig. S8. Comparison of energy efficiency between the NaMFM// hard carbon and NaLFM// hard carbon full cell at 50 mA g^{-1}, the full cell was precycled at 10 mA g^{-1}. Error bars: standard deviation of three cells for each sample.

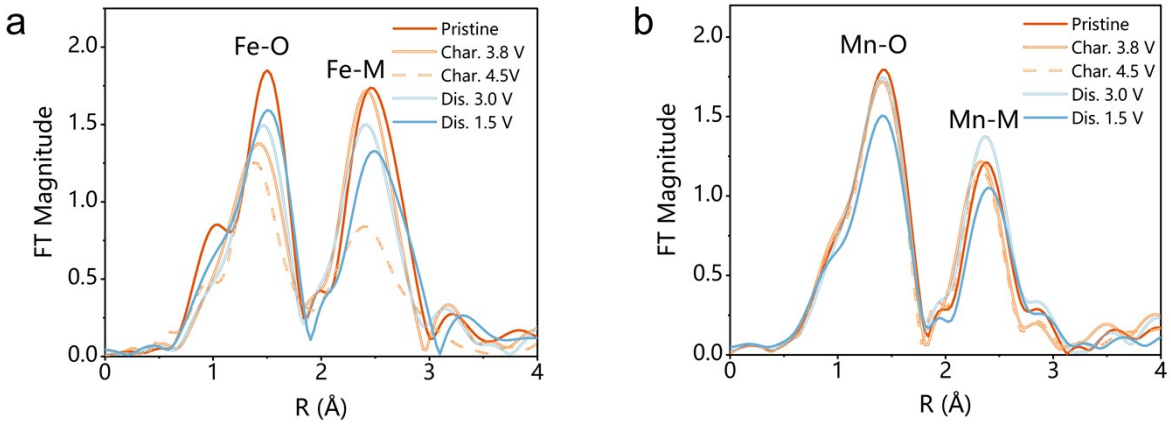

Fig. S9. EXAFS spectra at the (a) Fe K-edge and (b) Mn K-edge of NaLFM electrode collected at different charge/discharge states.

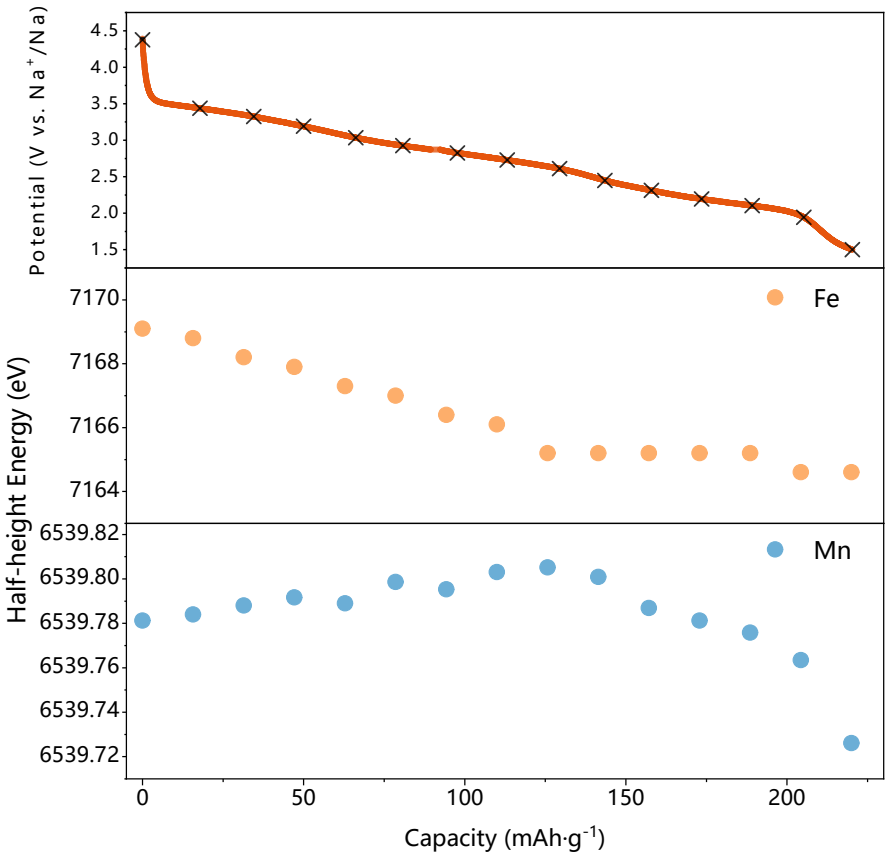

Fig. S10. The half-height changes of the in operando XANES at Fe K-edge and Mn pre-edge.

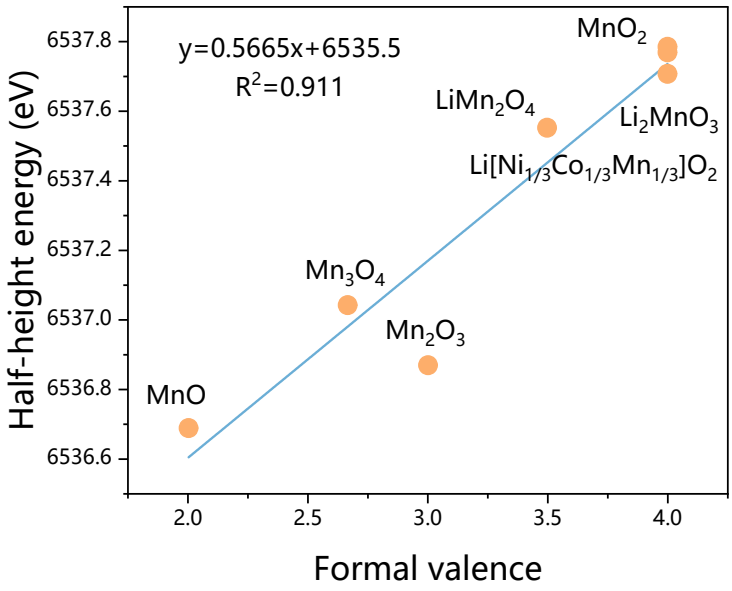

Fig. S11. Linear fit of the lower, pre-edge, half-height energy for the various sample standard valences.

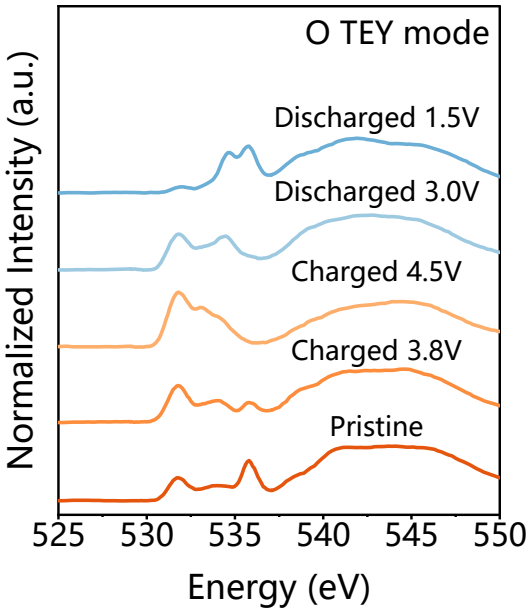

Fig. S12. TEY mode of oxygen K-edge soft XAS spectra at different states of NaLFM.

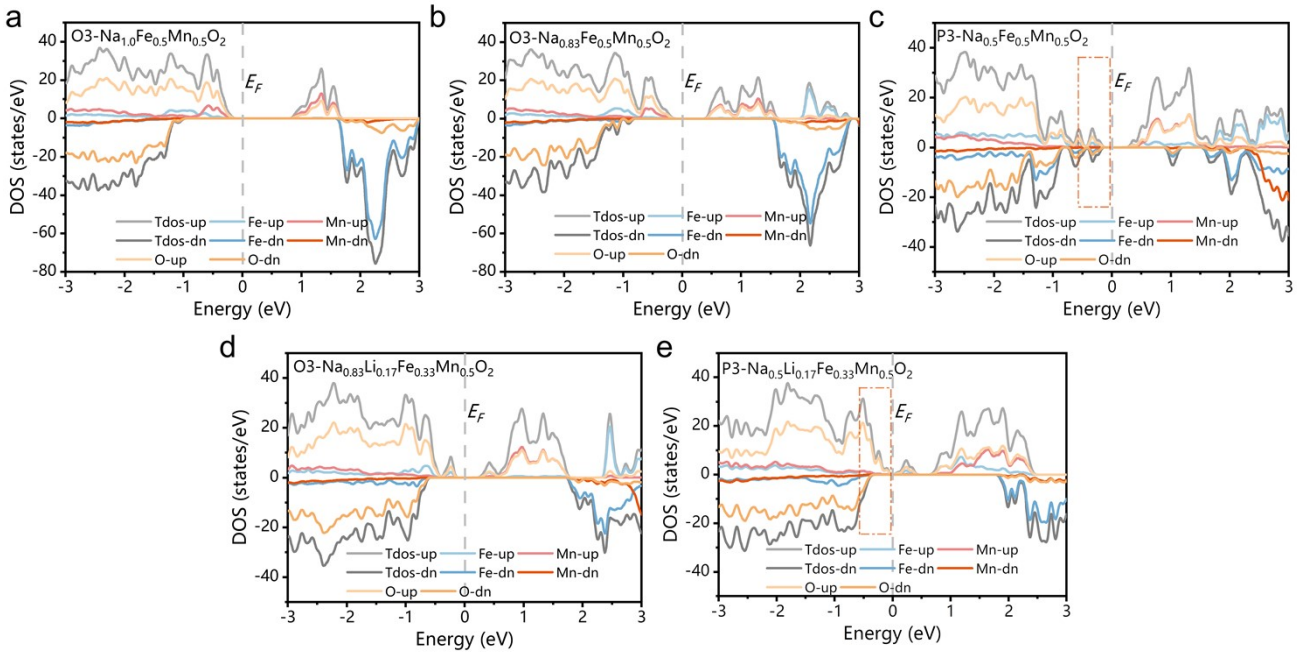

Fig. S13. Projected density of states (DOS) for various samples: (a-b) pristine $Na_{1.0}Fe_{0.5}Mn_{0.5}O_2$, $Na_{0.83}Li_{0.17}Fe_{0.33}Mn_{0.5}O_2$, and (c-e) charged samples $Na_{0.83}Fe_{0.5}Mn_{0.5}O_2$, $Na_{0.5}Fe_{0.5}Mn_{0.5}O_2$, and $Na_{0.5}Li_{0.17}Fe_{0.33}Mn_{0.5}O_2$. the electronic density of states (DOS) marked in the red dotted boxes is primarily composed of O p orbital characters. Comparing the DOS of $Na_{0.5}Fe_{0.5}Mn_{0.5}O_2$ and $Na_{0.5}Li_{0.17}Fe_{0.33}Mn_{0.5}O_2$, it is evident that the DOS contributed by O p orbitals just below the Fermi level in $Na_{0.5}Li_{0.17}Fe_{0.33}Mn_{0.5}O_2$ is significantly larger than that in $Na_{0.5}Fe_{0.5}Mn_{0.5}O_2$ (marked in the red dotted boxes). Furthermore, the DOS in $Na_{0.5}Li_{0.17}Fe_{0.33}Mn_{0.5}O_2$ is much closer to the Fermi level than that in $Na_{0.5}Fe_{0.5}Mn_{0.5}O_2$. These findings indicate the higher anionic redox activity of O2-/O- in $Na_{0.5}Li_{0.17}Fe_{0.33}Mn_{0.5}O_2$, contributing to the additional specific capacity during the charging process in the Li-doped compound.

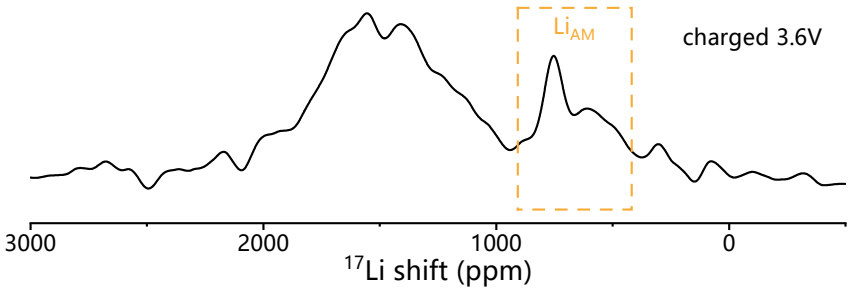

Fig S14. ^{7}Li pj-MATPASS NMR spectra of NaLFM charged to 3.6 V during the first cycle, the Li_{AM} signal still exists, which may be due to the presence of a small amount of O-type stacking faults within the P3 phase. The MAS frequency is 30 kHz for ^{7}Li NMR.

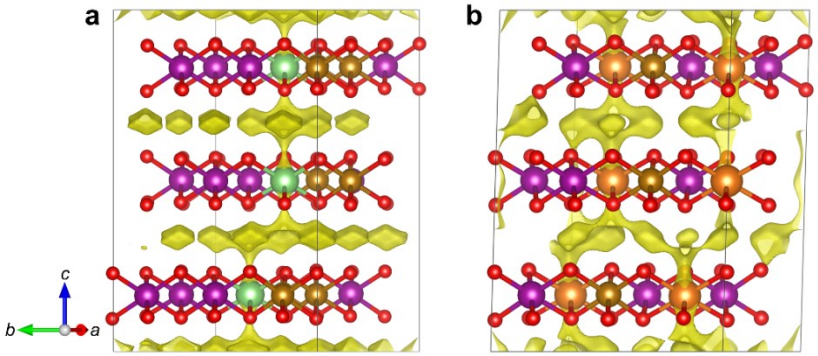

Fig S15. The BV calculations for de-sodiated (a) O3-$Na_{0.83}Li_{0.17}Fe_{0.33}Mn_{0.5}O_2$ (NaLFM) and (b) $Na_{0.83}Mg_{0.33}Fe_{0.17}Mn_{0.5}O_2$ (NaMFM) systems. For NaMFM system, the calculations were based on the supercell obtained by 2 × 3 × 1 expansion of the conventional cell O3-$NaFeO_2$ (R-*3*m), including 15 Na, 6 Mg, 3 Fe, 9 Mn and 36 O atoms.

To investigate the migration flexibility of Li and Mg ions, we conducted Bond Valence (BV) calculations for de-sodiated $Na_{0.83}Li_{0.17}Fe_{0.33}Mn_{0.5}O_2$ (NaLFM) and $Na_{0.83}Mg_{0.33}Fe_{0.17}Mn_{0.5}O_2$ (NaMFM) systems. The calculations indicate that the activation energy for Li in the NaLFM system is 1.6 eV, whereas for Mg in the NaMFM system it is 2.6 eV. This suggests that Li ions tend to migrate more readily than Mg ions.

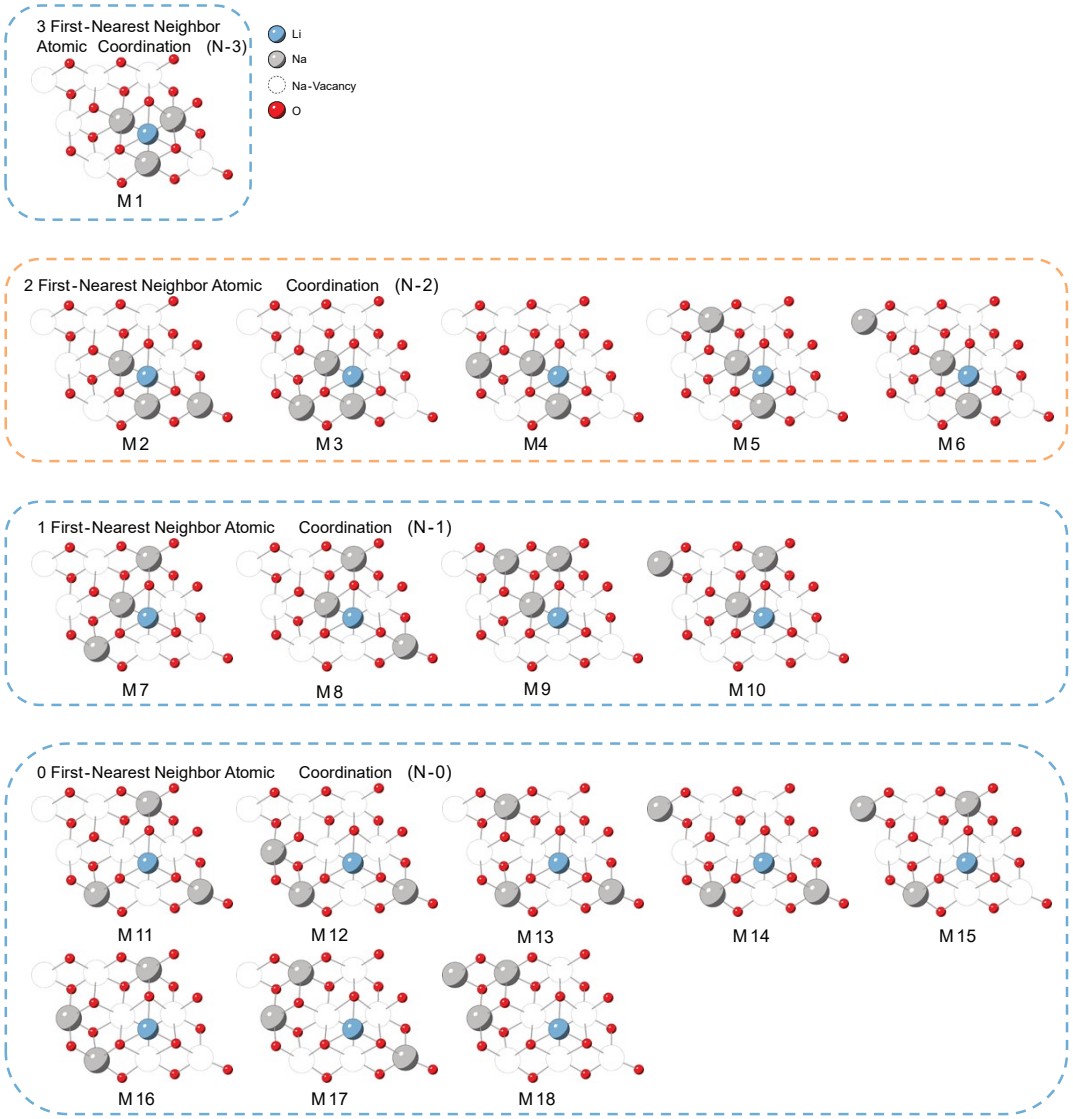

Fig. S16. Illustration of 18 configurations for $Na_{0.33}Li_{0.17}Fe_{0.33}Mn_{0.5}O_2$ under four different Na arrangement scenarios (N-3, N-2, N-1, and N-0)

In addition to $Na_{0.33}Li_{0.17}Fe_{0.33}Mn_{0.5}O_2$, we evaluated the suitability of N-3, N-2, N-1 and N-0 configurations across varying Na contents, including $Na_{0.22}Li_{0.17}Fe_{0.33}Mn_{0.5}O_2$ and $Na_{0.44}Li_{0.17}Fe_{0.33}Mn_{0.5}O_2$. Following structure optimization, it was observed that in all instances involving N-3, N-1, and N-0 configurations, Li ions were capable of returning to the transition metal layer. Conversely, in N-2 configurations, Li ions remained within the Na layer. Importantly, the energy levels of most N-3, N-1, and N-0 configurations were lower than those of N-2, consistent with the results obtained for $Na_{0.33}Li_{0.17}Fe_{0.33}Mn_{0.5}O_2$.This observation strongly suggests that the introduction of Li ions not only hinders the migration of Fe ions but also enhances the structural stability of the electrode material.

Table S1. Chemical composition of O3-$Na_{0.83}Li_{0.17}Fe_{0.33}Mn_{0.5}O_2$ and O3-$Na_{0.83}Mg_{0.33}Fe_{0.17}Mn_{0.50}O_2$ obtained by ICP-AES

Theoretical chemical formula	Measured atomic ratio				
	Na	Fe	Mn	Li	Mg
$Na_{0.83}Li_{0.17}Fe_{0.33}Mn_{0.5}O_2$	0.83(8)	0.33(6)	0.5	0.16(7)	0
$Na_{0.83}Mg_{0.33}Fe_{0.17}Mn_{0.50}O_2$	0.82(1)	0.17(1)	0.5	0	0.35(1)

Table S2. Crystallographic data and atomic positions of the O3-$Na_{0.83}Mg_{0.33}Fe_{0.17}Mn_{0.50}O_2$ determined from Rietveld refinement of its X-ray diffraction pattern.

O3-$Na_{0.83}Mg_{0.33}Fe_{0.17}Mn_{0.50}O_2$						
Space group = R -3 m		R_{wp}=11.7 %		χ^2=1.60		
a = 2.94562Å	*b* =2.94562 Å	*c* =16.30951 Å				
Atom	Wyckoff position	x	y	z	occupancy	Biso
Na	3a	0	0	0	0.828)	1.458
Mg	3b	0	0	0.5	0.333	1.823
Fe	3b	0	0	0.5	0.166	1.823
Mn	3b	0	0	0.5	0.544	1.823
O	6c	0	0	0.22933	1.004	1.426

Table S3. Crystallographic data and atomic positions of the O3-$Na_{0.83}Li_{0.17}Fe_{0.33}Mn_{0.5}O_2$ determined from Rietveld refinement of its neutron diffraction pattern.

NPD refinement results						
Space group = R -3 m		R_{wp}=2.358%				
a = 2.93208 Å	*b* = 2.93208Å	*c* = 16.26079 Å				
Atom	Wyckoff position	x	y	z	occ	Uiso
Na	3a	0	0	0	0.831	0.04245
Li	3a	0	0	0	0.035	0.04245
Li	3b	0	0	0.5	0.132	0.02571
Fe	3b	0	0	0.5	0.334	0.02571
Mn	3b	0	0	0.5	0.509	0.02571
O	6c	0	0	0.23088	1.032	0.02964
nPDF refinement results						
Space group = R -3 m		R_w=17.753%				
a = 2.9445 Å	*b* = 2.9445 Å	*c* = 16.3372 Å				
Atom	Wyckoff position	*x*	*y*	*z*	occ	Uiso
Na	3a	0	0	0	0.831	0.03136
Li	3a	0	0	0	0.035	0.03136
Li	3b	0	0	0.5	0.132	0.02453
Fe	3b	0	0	0.5	0.331	0.024539
Mn	3b	0	0	0.5	0.496	0.02453
O	6c	0	0	0.23088	1.051	0.01969

Table S4. Chemical composition of O3-$Na_{0.83}Li_{0.17}Fe_{0.33}Mn_{0.5}O_2$ after 1, 2, and 50 cycles obtained by ICP-AES

Cycle number	Measured atomic ratio		
	Li	Fe	Mn
1	0.16(7)	0.33(4)	0.5
2	0.16(5)	0.33(2)	0.5
50	0.15(1)	0.33(0)	0.5